Front. Phys. 13(5), 130506 (2018)
https://doi.org/10.1007/s11467-018-0783-1

RESEARCH ARTICLE

Dynamics of clustering patterns in the Kuramoto model with unidirectional coupling

Xia Huang[1,2,†], Jin Dong[1], Wen-Jing Jia[3], Zhi-Gang Zheng[3], Can Xu[3,‡]

[1] *School of Mathematics and Physics, North China Electric Power University, Beijing 102206, China*
[2] *Cardiovascular Research Laboratories, Departments of Medicine and Biomathematics, David Geffen School of Medicine, University of California, Los Angeles, Los Angeles, CA 90095, USA*
[3] *Institute of Systems Science and College of Information Science and Engineering, Huaqiao University, Xiamen 361021, China*
Corresponding authors. E-mail: [†] *xhuang@ncepu.edu.cn,* [‡] *xucan@hqu.edu.cn*
Received March 22, 2018; accepted May 4, 2018

We study the synchronization transition in the Kuramoto model by considering a unidirectional coupling with a chain structure. The microscopic clustering features are characterized in the system. We identify several clustering patterns for the long-time evolution of the effective frequencies and reveal the phase transition between them. Theoretically, the recursive approach is developed in order to obtain analytical insights; the essential bifurcation schemes of the clustering patterns are clarified and the phase diagram is illustrated in order to depict the various phase transitions of the system. Furthermore, these recursive theories can be extended to a larger system. Our theoretical analysis is in agreement with the numerical simulations and can aid in understanding the clustering patterns in the Kuramoto model with a general structure.

Keywords synchronization, coupled phase oscillators, phase transition

PACS numbers 05.45.-a, 05.65.+b, 05.45.Xt, 89.75.-k

1 Introduction

In coupled nonlinear systems, some microscopical synchronous behaviors are exhibited when the inner elements compete or cooperate with each other. The study of these cooperative behaviors covers various fields, which range from physics to chemistry, biology, and social economy, and include the Josephson junction, laser, chemical oscillator, biological cluster, ecological evolution, nerve, and heart [1–7]. Further research shows that various coupled mechanisms have a significant influence on the synchronization generation and function realization of the system. Hence, the investigation of these synchronous behaviors under various coupled schemes has a great significance on the understanding of numerous self-organization phenomena.

The most famous mathematical model depicting synchronous behaviors was proposed by Kuramoto (1975), i.e., the Kuramoto model [8]. This model describes a system of limit cycle oscillators interacting through trigonometric functions where the system is near the Hopf bifurcation and the amplitude effect can be neglected. In this case, the spontaneous synchronous process is equivalent to the nonequilibrium phase transition. Owing to its analytical solvability, the Kuramoto model was adopted in several applications. In the past decades, the Kuramoto model along with its generalization have attracted wide attention, including the basic theory analysis and their correlative to practice [9].

The original Kuramoto model describes a population of coupled phase oscillators wherein the interactions among the units are global and uniform, and each oscillator is coupled with the mean field in such a situation. It is well known that, when the natural frequencies of phase oscillators satisfy a unimodal and symmetric distribution $g(\omega)$, the classical Kuramoto model undergoes a second-order phase transition with a critical coupling strength $K_c = 2/(\pi g(0))$, and correspondingly, the branch of the order parameter near the critical point follows a radical scaling law [10]. Furthermore, when some heterogenous elements are introduced into the coupling strength, several novel synchronous states emerge; for example, a frequency-weighted coupling can result in Bellerophon

states [11, 12]; an abrupt phase transition to synchronization [13–17]; repulsive and attractive coupling can induce the occurrence of travelling and standing wave states, i.e., the Landau damping effect [18]; nonlocal coupling can result in chimera states [19–25]; and a time-shift or network structure coupling can result in nontrivial dynamical features in the limit-cycle system [26–28]. However, when local coupling is considered, the Kuramoto model can present a series of nontrivial collective dynamical behaviors; for instance, a novel single clustering synchronization in a ring of Kuramoto oscillators gives rise to a very small critical coupling strength K_c even if the oscillator number is large [29, 30]; a richness of solutions of nearest-neighbor Kuramoto-like coupled oscillators placed in a ring is studied above the critical synchronization transition [31, 32]; a modified Kuramoto model of synchronization in a finite discrete system of locally coupled oscillators is studied [31]; and synchronization in finite linear chains of oscillators has been investigated with nearest-neighbor coupling in a number of studies [33–37]. In this research, we study a unidirectional local coupling having a chain structure in the Kuramoto model. We found that all the effective frequencies of the phase oscillator are equal to the driving frequency in the synchronization regime while abundant competitive behaviors exist in the desynchronization regime. In particular, we analyze the special case that the number of oscillators $N = 3$, and four types of synchronization patterns are revealed for which the driving frequency is varied theoretically. Furthermore, the results of the finite size can be promoted to the system with larger size; all the numerical simulations are consistent with our theoretical analysis.

This paper is organized as follows. In the next section, we briefly introduce the unidirectional local coupling model having a chain structure and discuss the bifurcation diagrams obtained from the numerical simulations. In the third section, we perform a theoretical analysis of the special case in which $N = 3$ and generalize the results for larger systems. Finally, we summarize our work in the final section.

2 Numerical results of bifurcation diagrams

The dynamics of unidirectional coupled phase oscillators having a chain structure can be described using the following equations.

$$\begin{cases} \dot{\theta}_1 = \omega_1 \\ \dot{\theta}_i = \omega_i + \lambda \sin(\theta_{i-1} - \theta_i), \quad i = 2, 3, \cdots, N, \end{cases} \tag{1}$$

where the dot denotes the time derivation, θ_i is the phase of the i-th oscillator, ω_i is the natural frequency, which is selected from a random sequence, and $\lambda > 0$ is the coupling strength among the units. The significant characteristic of the current model is that the coupling pattern is unidirectional with a chain structure as shown in Fig. 1. Therefore, θ_1 is the driving source that oscillates with the natural frequency ω_1, whereas the other oscillators interact with their neighbor on the left. In order to characterize the degree of synchronization, the microscopic effective frequencies can be defined as follows.

Fig. 1 Diagram of chain structure wherein oscillator 1 is the driving source, the other $N-1$ oscillators are the driven oscillators, and the arrows represent a unidirectional coupling.

$$\Omega_i = \lim_{T\to\infty} \frac{1}{T} \int_0^T \dot{\theta} \mathrm{d}t, \tag{2}$$

when all the oscillators share a common value, it indicates that a total synchronization of the system has occurred. However, Ω_i behaves like a random form, which implies that the system is in a completely disordered state, i.e., an incoherent state.

Bifurcation diagrams of the effective frequencies with the coupling strength are illustrated in Fig. 2; without the loss of generality, the system is assumed to be of a finite size $N = 6$. It has been proved that the effective frequency of the second oscillator can be derived from Eq. (1). Therefore, we can fix the natural frequencies $\omega_1 = 2$ and $\omega_2 = 1$ without restricting the others. As mentioned above, all the oscillators have a common effective frequency in the synchronous regime, which is equal to the driving source ω_1. Typically, there are four types of clustering patterns in the regime that occurs before the critical point when the coupling strength is increased. For the first case, we find that the oscillator synchronizes with its driving neighbor to form a local cluster, and the local cluster then joins the other group with an increase in the coupling strength, as in the case of oscillator 3, which is shown in Figs. 2(a), (c), and (d), and oscillator 4 shown in Figs. 2(b)–(d). For the second case, it is shown that the driven oscillator first synchronizes with the driving source, and it is then phase-locked with its driving neighbor as in the case of oscillator 6 shown in Fig. 2(a) and oscillators 3 and 5 shown in Fig. 2(b). In the third case, when the coupling strength is sufficiently small, we find that the oscillator synchronizes with the driving neighbor, thus forming a local cluster. However, this small group is dissolved with an increase in λ, which is indicated by different effective frequencies. This desynchronous phenomenon is exhibited by oscillator 5 in Fig. 2(d). Finally, the driving oscillator is phase-locked with the source and then synchronizes with the driven oscillator: for example, oscillator 6 in

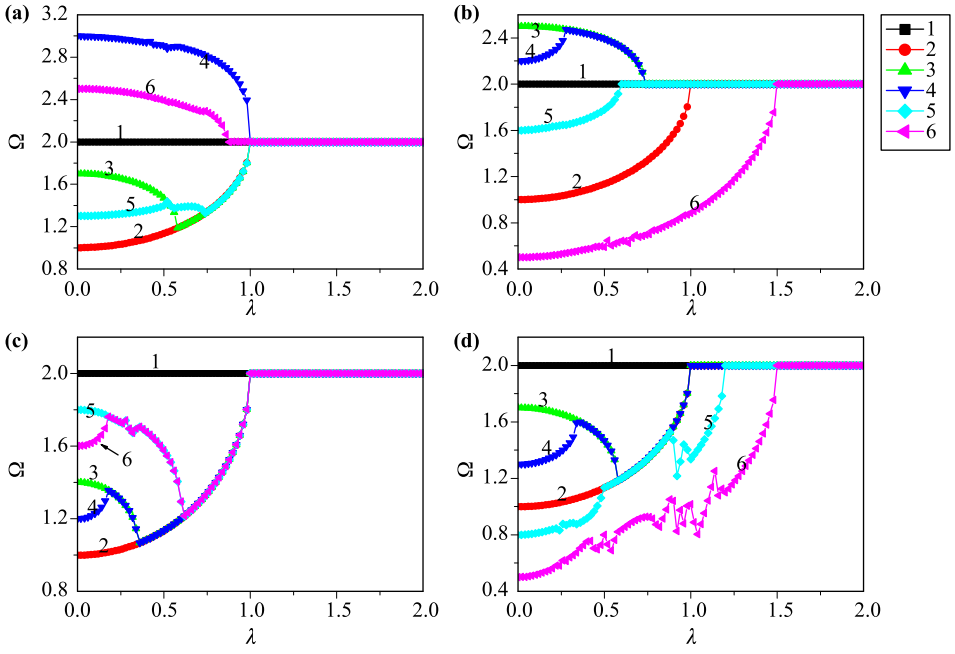

Fig. 2 Bifurcation diagram (Ω versus λ) characterizing the forward clustering transitions in model (1) with different frequency arrangements, where the horizontal axis represents the coupling strength λ, the vertical axis represents the effective frequency Ω, and the finite size $N = 6$. The effective frequencies of the first and second oscillators are fixed as $\omega_1 = 2$ and $\omega_2 = 1$ without restricting the other frequencies. There are four types of clustering patterns in the regime that occurs before the critical point when the coupling strength is increased.

Figs. 2(b) and (d). The aforementioned clustering patterns are universal in the route to synchronization with generalized network structures. Therefore, it is necessary for us to understand the bifurcation mechanism of this system. We perform a theoretical analysis of the effective frequencies and address this issue in the following section.

3 Theoretical analysis

In order to obtain some analytical insights of the dynamical features of the aforementioned system, we explore the bifurcation scheme of the effective frequencies for a system of finite size having a chain structure. Specifically, we assume that the size of the system is $N = 3$, and $\omega_1 = 2$ and $\omega_2 = 1$. Generally, the four types of clustering patterns in Section 2 can be found in a small system with various arrangements of the natural frequency ω_3. We focus on limiting the values of ω_3 in four different intervals. First, when $\omega_3 \in [1, 2]$, Fig. 3(a) shows that oscillator 3 has its effective frequency close to that of the driving oscillator 2 regardless of its specific position in the interval. When the coupling strength is sufficiently large, this cluster synchronizes with the driving source that corresponds to the first case in Section 2. Second, when $\omega_3 \in (2, 3]$, Fig. 3(b) points out that oscillator 3 tends to be consistent with the driving source instead of its neighbor. For a special case in which $\omega_3 = 3$, the phase transition takes place at a common critical coupling strength, which is in accordance with the second case in Section 2. Third, when ω_3 is close to 1, Fig. 3(c) illustrates that oscillator 3 coincides with the driving oscillator 2 in the small coupling strength regime, but the group is broken owing to the increasing value of λ, and as a result, this bifurcation is similar to the third case in Section 2. Finally, when ω_3 is far from ω_1 and ω_2, it is found that the driving oscillator 2 joins the source at a small coupling strength to form a local cluster, and the driven oscillator 3 is then entrained by the cluster at a larger λ in Fig. 3(d), and this process follows the same path as that of the last case in Section 2.

We start with an approximate analysis of the bifurcation diagram; for a system wherein $N = 3$, the dynamic model can be written as

$$\begin{cases} \dot{\theta}_1 = \omega_1 \\ \dot{\theta}_2 = \omega_2 + \lambda \sin(\theta_1 - \theta_2) \\ \dot{\theta}_3 = \omega_3 + \lambda \sin(\theta_2 - \theta_3). \end{cases} \tag{3}$$

The evolution of the phase difference $\phi_{21} = \theta_2 - \theta_1$ is governed by

$$\dot{\phi}_{21} = \Delta\omega_{21} - \lambda \sin \phi, \tag{4}$$

where $\Delta\omega_{21} = \omega_2 - \omega_1$. Without the loss of generality, we let $\Delta\omega_{21} \geq 0$, and the effective frequency of oscillator 2 is

$$\langle \dot{\theta}_2 \rangle = \omega_2 - \lambda \langle \sin \phi_{21} \rangle. \tag{5}$$

Here, the symbol $\langle \cdot \rangle$ denotes the time average. In the long-time limit, the time average can be replaced by the ensemble average over the system. Consequently, for a small λ, the phase difference ϕ_{21} can never reach a fixed point but varies in the interval $[0, 2\pi]$ non-uniformly. Furthermore, a probability density function $\rho(\phi_{21}, t)$ is introduced. In the long term, $\rho(\phi_{21}, t)$ approaches a stationary

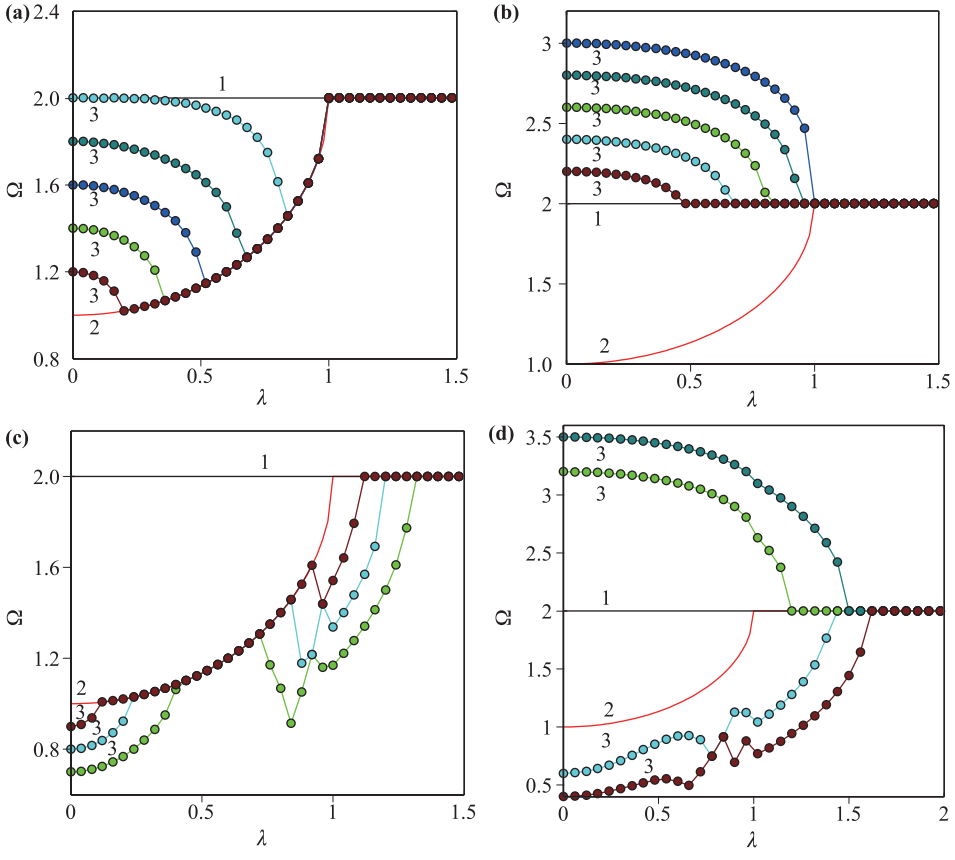

Fig. 3 Typical four examples of bifurcation diagrams (Ω versus λ) characterizing the forward clustering transitions with a finite size $N = 3$, where $\omega_1 = 2$ and $\omega_2 = 1$ are fixed, and the value of ω_3 is random. **(a)** $\omega_2 < \omega_3 < \omega_1$ represents type one, **(b)** $\omega_1 < \omega_3 < \omega_1 + \Delta_{12}$ represents type two, **(c)** $(1-\sqrt{2})\omega_1 + \sqrt{2}\omega_2 < \omega_3 < \omega_2$ represents type three, and **(d)** $\omega_3 > \omega_1 + \Delta\omega_{12}$ and $\omega_3 < (1-\sqrt{2})\omega_1 + \sqrt{2}\omega_2$ represent type four, where $\omega_{12} = \omega_1 - \omega_2 = 1$.

state:

$$\rho(\phi_{21}, t) = \frac{\Delta\omega_{21} - \lambda \sin\phi_{21}}{C}, \tag{6}$$

where $C = \sqrt{(\Delta\omega_{21})^2 - \lambda^2}$ is a normalization constant. Therefore, in the regime before the phase transition,

$$\langle \sin\phi_{21} \rangle = \int_0^{2\pi} \frac{\sin\phi_{21} \cdot C}{\Delta\omega_{21} - \lambda\sin\phi_{21}} \mathrm{d}\phi_{21}, \tag{7}$$

which can be calculated using the residue theorem, which yields

$$\langle \sin\phi_{21} \rangle = \frac{\Delta\omega_{21} - \sqrt{(\Delta\omega_{21})^2 - \lambda^2}}{\lambda}. \tag{8}$$

On substituting Eq. (8) into Eq. (5), one obtains the effective frequency of θ_2.

$$\langle \dot{\theta}_2 \rangle = \omega_1 + \sqrt{(\Delta\omega_{21})^2 - \lambda^2}. \tag{9}$$

This is an intuitive result that is consistent with the actual condition; when $\lambda = 0$, $\langle \dot{\theta}_2 \rangle = \omega_2$. With the increase in λ, $\langle \dot{\theta}_2 \rangle$ gradually moves closer to ω_1; at a critical point $\lambda_c = \Delta\omega$, $\langle \dot{\theta}_2 \rangle = \omega_1$, which indicates a phase-locked state. It should be noted that the same strategy can be adopted for the case of $\Delta\omega_{21} < 0$; in this situation, the normalization constant C is negative, and the effective frequency of θ_2 can be replaced as follows:

$$\langle \dot{\theta}_2 \rangle = \omega_1 - \sqrt{(\Delta\omega_{21})^2 - \lambda^2}. \tag{10}$$

We then investigate the effective frequency of θ_3 with the framework of $\langle \dot{\theta}_2 \rangle$. Similarly, by introducing the phase difference $\phi_{32} = \theta_3 - \theta_2$, the dynamical evolution of ϕ_{32} reads as

$$\dot{\phi}_{32} = \omega_3 - \dot{\theta}_2 - \lambda \sin\phi_{32}. \tag{11}$$

For the long-time limit ($t \to \infty$), the instantaneous velocity of θ_2 can be approximately replaced by the asymptotic solution of $\langle \dot{\theta}_2 \rangle$. Accordingly, the effective frequency of θ_3 can be calculated in a similar manner:

$$\langle \dot{\theta}_3 \rangle = \langle \dot{\theta}_2 \rangle \pm \sqrt{(\Delta\omega_{32})^2 - \lambda^2}, \tag{12}$$

where $\Delta\omega_{32} = \omega_3 - \langle \dot{\theta}_2 \rangle$. If $\Delta\omega_{32} > 0$, the second term of Eq. (12) should be positive; conversely, if $\Delta\omega_{32} < 0$, it is negative. We emphasize here that the validity of the effective frequencies must ensure that the terms in the radical are positive.

According to the effective frequency of Eq. (12), we obtain the phase-locked condition for θ_3 and θ_2, that is, $|\Delta\omega_{32}| \le \lambda$. Considering the expression of $\langle \dot{\theta}_2 \rangle$, if $\Delta\omega_{21} \ge$

0, the condition of synchronization between oscillators 3 and 2 becomes

$$\begin{cases} -\lambda \le \Delta\omega_{31} - \sqrt{(\Delta\omega_{21})^2 - \lambda^2} \le \lambda, & (\lambda \le \lambda_c) \\ -\lambda \le \Delta\omega_{31} \le \lambda, & (\lambda > \lambda_c), \end{cases} \tag{13}$$

and if $\Delta\omega_{21} < 0$, the condition of synchronization between oscillators 3 and 2 is

$$\begin{cases} -\lambda \le \Delta\omega_{31} + \sqrt{(\Delta\omega_{21})^2 - \lambda^2} \le \lambda, & (\lambda \le \lambda_c) \\ -\lambda \le \Delta\omega_{31} \le \lambda, & (\lambda > \lambda_c), \end{cases} \tag{14}$$

where $\lambda_c = |\Delta\omega_{21}|$, and $\Delta\omega_{31} = \omega_3 - \omega_1$.

Fig. 4 depicts the phase graphics of the natural frequency ω_3 and coupling strength λ for the case in which $\Delta\omega_{21} < 0$. It has been proven that in the area wherein $\lambda > \lambda_c$, oscillator 2 is always phase-locked with the driving source while oscillator 3 only synchronizes with oscillator 2 in the yellow trapezium region. The red boundary lines are determined from the second expression in Eq. (14). For a low coupling strength, that is, $\lambda < \lambda_c$, the phase-locked area between oscillators 2 and 3 is covered by the green fan-shaped regime, wherein the two parabolic boundary lines may be solved using the first expression in Eq. (14). These analyses can aid in explaining the desynchronization scheme between oscillators 2 and 3. When $\omega_3 \in (\omega_c, \omega_2)$, the critical frequency $\omega_c = -\sqrt{2}|\Delta\omega_{21}| + \omega_1$ is the line that is tangent to the parabolic in the lower branch, and the desynchronization occurs once λ goes through the green area characterized by the dispersive effective frequencies $\langle\dot{\theta}_2\rangle$ and $\langle\dot{\theta}_3\rangle$.

The previous numerical simulations reveal that, for the second clustering pattern, $\omega_3 > \omega_1$, where oscillator 3

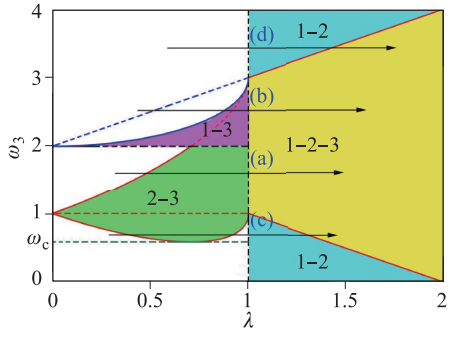

Fig. 4 Phase diagram for the natural frequency ω_3 and coupling strength λ for the case wherein $\omega_1 = 2$ and $\omega_2 = 1$. The arrows (a)–(d) correspond to four types of clustering patterns in Figs. 3(a)–(d). In the area wherein $\lambda > \lambda_c$, oscillator 2 is always phase-locked with the driving source while oscillator 3 only synchronizes with oscillator 2 in the yellow trapezium region. For the small coupling strength $\lambda < \lambda_c$, the phase-locked area between oscillator 2 and oscillator 3 is covered by the green fan-shaped regime, and oscillator 3 can synchronize with the driving source directly in the purple area.

can synchronize with the driving source directly. Hence, it is necessary to achieve the synchronization conditions between oscillator 3 and the driving source by using a similar strategy that involves introducing the phase difference $\phi_{31} = \theta_3 - \theta_1$. The dynamical evolution of ϕ_{31} can be expressed as

$$\dot{\phi}_{31} = \Delta\omega_{31} - \lambda\sin(\phi_{31} - \phi_{21}). \tag{15}$$

From Eq. (15), it is observed that the necessary phase-locked conditions for θ_3 and θ_1 is $|\Delta\omega_{31}| \le \lambda$. In addition, when the effective frequency $\langle\dot{\theta}_3\rangle = \omega_1$, the sufficient phase-locked condition can be obtained from Eq. (12), which yields

$$\omega_3 = \omega_1 + |\Delta\omega_{21}| - \sqrt{(\Delta\omega_{21})^2 - \lambda^2}. \tag{16}$$

The corresponding phase-locked condition is represented by the purple area in Fig. 4. The four types of clustering patterns in Figs. 3(a)–(d) are illustrated by the arrows (a)–(d) in Fig. 4.

For a system of a finite size ($N \gg 3$), the effective frequency of the i-th oscillator can be analogized using the following recursive equation:

$$\langle\dot{\theta}_i\rangle = \langle\dot{\theta}_{i-1}\rangle \pm \sqrt{(\Delta\omega_{i,i-1})^2 - \lambda^2}, \tag{17}$$

where $\Delta\omega_{i,i-1} = \omega_i - \langle\dot{\theta}_{i-1}\rangle$. On combining this with the phase-locked conditions $|\Delta\omega_{i,i-1}| \le \lambda$, the clustering pattern can be preliminarily predicted. Furthermore, some additional limitations owing to which the driven i-th oscillator can coincide with the indirect driving oscillators should be taken into consideration. The necessary and sufficient condition for this restriction is as follows.

$$\langle\dot{\theta}_i\rangle = \langle\dot{\theta}_{i'}\rangle, \quad i' = 1, 2, \ldots, i-2. \tag{18}$$

With Eqs. (17) and (18), the clustering patterns or the bifurcation scheme of the system before the synchronous regime can be formally predicted. Fig. 5 shows an example of $N = 10$ with various arrangements of natural frequencies, and the rich clustering figures between the oscillators are observed, which can be further understood in terms of the aforementioned theoretical framework.

4 Conclusion

In this study, we extend the classical Kuramoto model in a chain structure with unidirectional coupling, wherein the oscillators are driven by the neighbor on the left. For a system of finite size, the numerical simulations reveal that the system can exhibit rich clustering features before the synchronous regime for various combinations of natural frequencies. The regular synchronization, indirect synchronization, and desynchronization are charac-

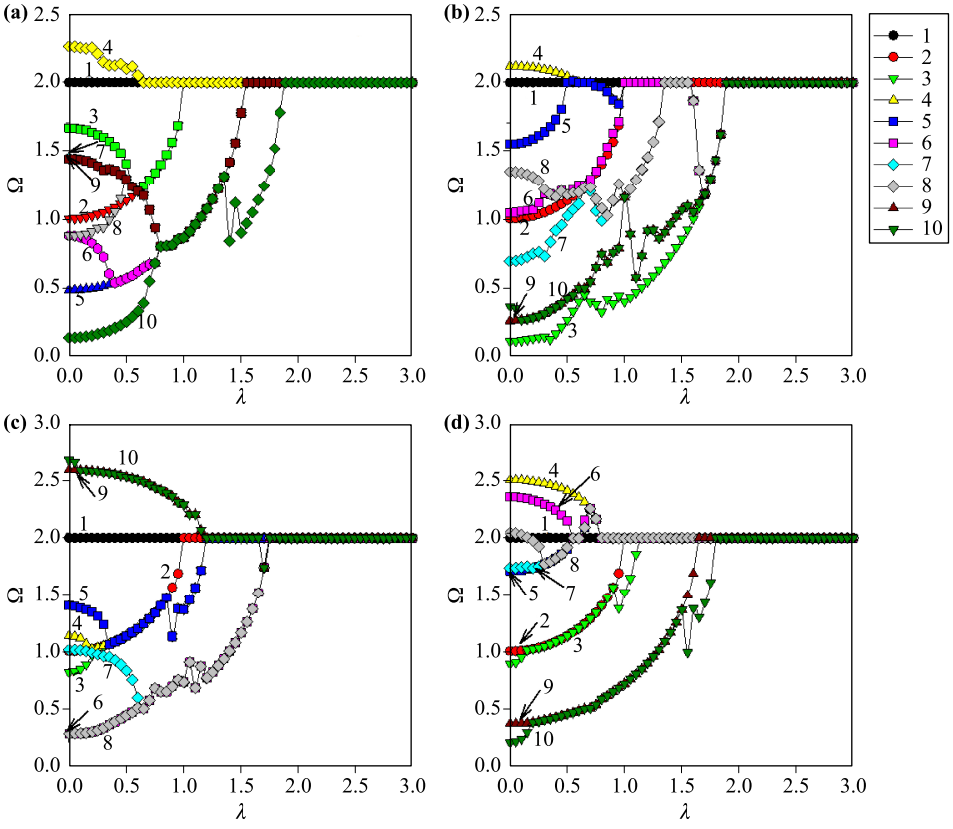

Fig. 5 Bifurcation diagrams (Ω versus λ) for characterizing the forward clustering transitions with a finite system size of $N = 10$, where $\omega_1 = 2$ and $\omega_2 = 1$ are fixed, and the frequencies of oscillators 3–10 are random. There are four types of clustering patterns in the regime that occurs before the critical point when the coupling strength is increased.

terized in the bifurcation diagrams of the effective frequencies. Theoretically, the recursive equations are developed to reveal the bifurcation schemes of the effective frequencies, and a phase diagram is used to illustrate the conversions among the clustering patterns. In addition, these analyses can be generalized to a system of a larger size. These results aid in the comprehension of the complicated collective behavior in the Kuramoto model with generalized structures.

Acknowledgements This work was supported partly by the National Natural Science Foundation of China (Grant Nos. 11605055 and 11475022), the Fundamental Research Funds for the Central Universities of China (Grant No. 2017MS054), and the Scientific Research Funds of Huaqiao University (Grant Nos. 600005-Z17Y0064 and 15BS401) and China Scholarship Council (CSC).

References

1. A. Pikovsky, M. Rosenblum, and J. Kurths, Synchronization: A Universal Concept in Nonlinear Sciences, Vol. 12, Cambridge: Cambridge University Press, 2003
2. S. H. Strogatz, Frontiers in Mathematical Biology, Springer, 2012, pp 122–138
3. J. A. Mohawk, C. B. Green, and J. S. Takahashi, Central and peripheral circadian clocks in mammals, *Annu. Rev. Neurosci.* 35(1), 445 (2012)
4. Z. Qu, Y. Shiferaw, and J. N. Weiss, Nonlinear dynamics of cardiac excitation-contraction coupling: an iterated map study, *Phys. Rev. E* 75(1), 011927 (2007)
5. I. Aihara, Modeling synchronized calling behavior of Japanese tree frogs, *Phys. Rev. E* 80(1), 011918 (2009)
6. S. H. Strogatz, Sync: How Order Emerges from Chaos in the Universe, Nature and Daily Life, UK: Hachette, 2004
7. B. C. Daniels, S. T. M. Dissanayake, and B. R. Trees, Synchronization of coupled rotators: Josephson junction ladders and the locally coupled Kuramoto model, *Phys. Rev. E* 67(2), 026216 (2003)
8. Y. Kuramoto and H. Araki, Lecture notes in physics, International Symposium on Mathematical Problems in Theoretical Physics, 5 (1975)
9. J. A. Acebrón, L. L. Bonilla, C. J. P. Vicente, et al., The Kuramoto model: A simple paradigm for synchronization phenomena, *Rev. Mod. Phys.* 77(1), 137 (2005)
10. C. Xu, J. Gao, H. Xiang, W. Jia, S. Guan, and Z. Zheng, Dynamics of phase oscillators with generalized frequency-weighted coupling, *Phys. Rev. E* 94(6), 062204 (2016)
11. H. Bi, X. Hu, S. Boccaletti, X. Wang, Y. Zou, Z. Liu, and S. Guan, Coexistence of quantized, time dependent, clusters in globally coupled oscillators, *Phys. Rev. Lett.* 117(20), 204101 (2016)

12. X. Huang, J. Gao, Y. Sun, Z. Zheng, and C. Xu, Effects of frustration on explosive synchronization, *Front. Phys.* 11(6), 110504 (2016)
13. S. Boccaletti, J. A. Almendral, S. Guan, I. Leyva, Z. Liu, I. Sendiña-Nadal, Z. Wang, and Y. Zou, Explosive transitions in complex networks structure and dynamics: Percolation and synchronization, *Phys. Rep.* 660, 1 (2016)
14. H. Chen, Y. Sun, J. Gao, Z. Zheng, and C. Xu, Order parameter analysis of synchronization transitions on star networks, *Front. Phys.* 12(6), 120504 (2017)
15. X. Zhang, X. Hu, J. Kurths, and Z. Liu, Explosive synchronization in a general complex network, *Phys. Rev. E* 88(1), 010802 (2013)
16. X. Zhang, S. Boccaletti, S. Guan, and Z. Liu, Explosive synchronization in adaptive and multilayer networks, *Phys. Rev. Lett.* 114(3), 038701 (2015)
17. H. Bi, Y. Li, L. Zhou, and S. Guan, Nontrivial standing wave state in frequency-weighted Kuramoto model, *Front. Phys.* 12(3), 126801 (2017)
18. T. Qiu, Y. Zhang, J. Liu, H. Bi, S. Boccaletti, Z. Liu, and S. Guan, Landau damping effects in the synchronization of conformist and contrarian oscillators, *Sci. Rep.* 5(1), 18235 (2016)
19. G. C. Sethia, A. Sen, and F. M. Atay, Clustered chimera states in delay-coupled oscillator systems, *Phys. Rev. Lett.* 100(14), 144102 (2008)
20. Y. Zhu, Y. Li, M. Zhang, and J. Yang, The oscillating two-cluster chimera state in non-locally coupled phase oscillators, *Europhys. Lett.* 97(1), 10009 (2012)
21. D. M. Abrams, R. Mirollo, S. H. Strogatz, and D. A. Wiley, Solvable model for chimera states of coupled oscillators, *Phys. Rev. Lett.* 101(8), 084103 (2008)
22. O. E. Omel'chenko, M. Wolfrum, S. Yanchuk, Y. L. Maistrenko, and O. Sudakov, Stationary patterns of coherence and incoherence in two-dimensional arrays of non-locally-coupled phase oscillators, *Phys. Rev. E* 85(3), 036210 (2012)
23. J. Sieber, E. Omel'chenko, and M. Wolfrum, Controlling unstable chaos: Stabilizing chimera states by feedback, *Phys. Rev. Lett.* 112(5), 054102 (2014)
24. B. K. Bera, S. Majhi, D. Ghosh, and M. Perc, Chimera states: Effects of different coupling topologies, *Europhys. Lett.* 118(1), 10001 (2017)
25. S. Rakshit, B. K. Bera, M. Perc, and D. Ghosh, Basin stability for chimera states, *Sci. Rep.* 7(1), 2412 (2017)
26. E. Bolhasani, Y. Azizi, A. Valizadeh, and M. Perc, Synchronization of oscillators through timeshifted common inputs, *Phys. Rev. E* 95(3), 032207 (2017)
27. Q. Wang, Z. Duan, M. Perc, and G. Chen, Synchronization transitions on small-world neuronal networks: Effects of information transmission delay and rewiring probability, *Europhys. Lett.* 83(5), 50008 (2008)
28. Q. Wang, M. Perc, Z. Duan, and G. Chen, Synchronization transitions on scale-free neuronal networks due to finite information transmission delays, *Phys. Rev. E* 80(2), 026206 (2009)
29. Y. Wu, J. Xiao, G. Hu, and M. Zhan, Synchronizing large number of nonidentical oscillators with small coupling, *Europhys. Lett.* 101, 38002 (2013)
30. X. Huang, M. Zhan, F. Li, and Z. Zheng, Single clustering synchronization in a ring of Kuramoto oscillators, *J. Phys. A* 47(12), 125101 (2014)
31. P. F. C. Tilles, F. F. Ferreira, and H. A. Cerdeira, Multistable behavior above synchronization in a locally coupled Kuramoto model, *Phys. Rev. E* 83(6), 066206 (2011)
32. Y. Zhang and W. Wan, States and transitions in mixed networks, *Front. Phys.* 9(4), 523 (2014)
33. L. Ren and B. Ermentrout, Phase locking in chains of multiple-coupled oscillators, *Physica D* 143(1–4), 56 (2000)
34. L. Ren and G. B. Ermentrout, Monotonicity of phase-locked solutions in chains and arrays of nearest-neighbour coupled oscillators, *SIAM J. Math. Anal.* 29(1), 208 (1998)
35. J. A. Rogge and D. Aeyels, Stability of phase locking in a ring of unidirectionally coupled oscillators, *J. Phys. Math. Gen.* 37(46), 11135 (2004)
36. H. F. El-Nashar and H. A. Cerdeira, Determination of the critical coupling for oscillators in a ring, *Chaos* 19(3), 033127 (2009)
37. G. B. Ermentrout, The behaviour of rings of coupled oscillators, *J. Math. Biol.* 23(1), 55 (1985)